

Characteristics of the xenon plasma sustained by lasers in different incidence directions

Yanfei Hu(胡艳菲), Valeria Borodina, Vladimir Sukhomlinov, Nikolai Timofeev, Xinbing Wang(王新兵), Duluo Zuo(左都罗)

Citation: Chin. Phys. B. 35, 095201 (2026). DOI: 10.1088/1674-1056/ae1cb6 | CSTR: 32038.14.CPB.ae1cb6

http://cpb.iphy.ac.cn; http://iopscience.iop.org/cpb

What follows is a list of articles you may be interested in

Spatiotemporal pulse-shaping effects on 4-μm laser-driven Sn microdroplet plasmas for extreme ultraviolet emission

Qi Min(敏琦), Chunbo Miao(苗春波), Hongyu Liu(刘宏宇), Xingbang Liu(刘兴邦), Haidong Lu(卢海东), Maogen Su(苏茂根), Chenzhong Dong(董晨钟)

Chin. Phys. B. 35, 075203 (2026). DOI: 10.1088/1674-1056/ae74c1 | CSTR: 32038.14.CPB.ae74c1

Observation of Weibel magnetic fields in laser-produced interpenetrating flows

Chuanqi Shi(施川奇), Dawei Yuan(袁大伟), Wei Sun(孙伟), Yapeng Zhang(张雅芃), Zhijie Qiu(邱志杰), Huigang Wei(魏会冈), Zhe Zhang(张喆), Xiaohui Yuan(远晓辉), Gang Zhao(赵刚)

Chin. Phys. B. 34, 015203 (2025). DOI: 10.1088/1674-1056/ad94e4 | CSTR: 32038.14.CPB.ad94e4

Influence of crystal dimension on performance of spherical crystal self-emission imager

Chenglong Zhang(张成龙), Yihang Zhang(张翌航), Haochen Gu(谷昊琛), Nuo Chen(陈诺), Xiaohui Yuan(远晓辉), Zhe Zhang(张喆), Miaohua Xu(徐妙华), Yutong Li(李玉同), Yingjun Li(李英骏), Jie Zhang(张杰)

Chin. Phys. B. 33, 125205 (2024). DOI: 10.1088/1674-1056/ad84d2

Proton acceleration in plasma turbulence driven by high-energy lepton jets

Gaowei Zhang(张高维), Zhengming Sheng(盛政明), Suming Weng(翁苏明), Min Chen(陈民), Jie Zhang(张杰)

Chin. Phys. B. 33, 115203 (2024). DOI: 10.1088/1674-1056/ad7b01

Spectral characteristics of laser-plasma instabilities with a broadband laser

Guo-Xiao Xu(许国潇), Ning Kang(康宁), An-Le Lei(雷安乐), Hui-Ya Liu(刘会亚), Yao Zhao(赵耀), Shen-Lei Zhou(周申蕾), Hong-Hai An(安红海), Jun Xiong(熊俊), Rui-Rong Wang(王瑞荣), Zhi-Yong Xie(谢志勇), Xi-Chen Zhou(周熙晨), Zhi-Heng Fang(方智恒), Wei Wang(王伟)

Chin. Phys. B. 33, 085204 (2024). DOI: 10.1088/1674-1056/ad426d

---

Characteristics of the xenon plasma sustained by lasers in different incidence directions

Yanfei Hu(胡艳菲)[1], Valeria Borodina[2], Vladimir Sukhomlinov[2], Nikolai Timofeev[2], Xinbing Wang(王新兵)[1,†], and Duluo Zuo(左都罗)[1]

[1] *Wuhan National Laboratory for Optoelectronics, Huazhong University of Science and Technology, Wuhan* 430074, *China*
[2] *Department of Optics, Spectroscopy and Plasma Physics, Saint Petersburg State University, Saint Petersburg* 199034, *Russia*

(Received 1 September 2025; revised manuscript received 17 October 2025; accepted manuscript online 7 November 2025)

Xenon plasma was sustained using continuous fiber lasers with varying incident directions, and the stability of the plasma was analyzed through both experimental and theoretical approaches. High-speed cameras were employed to analyze the plasma's shape and size, while photodetectors recorded the plasma's brightness fluctuations. It was found that plasma sustained by lasers incident from below exhibited greater stability, as indicated by smaller standard deviations of the centroid and axial diameter, as well as reduced brightness fluctuation amplitudes. The Schlieren method revealed an upward circulating hot bubble surrounding the plasma. Fluid dynamic analysis of gas flows surrounding the high-temperature plasma demonstrated turbulent flow in the region above the plasma and laminar flow below it, as determined by Reynolds number evaluation. This observation provides a fundamental explanation for the superior stability observed in plasmas sustained by laser irradiation from below. A direct relationship between Kelvin–Helmholtz instability and the formation of toroidal vortex structures was confirmed. Based on combined experimental and simulation results, the optical configuration for plasma maintenance was optimized. By employing bottom laser irradiation with $F = 0.8$, a highly stable, small-diameter plasma with nearly perfect circular symmetry was achieved.

Keywords: laser sustained plasma, plasma instability, convection, fluctuation frequency

PACS: 52.50.Jm, 52.25.Os

DOI: 10.1088/1674-1056/ae1cb6 **CSTR:** 32038.14.CPB.ae1cb6

1. Introduction

Laser-sustained plasma (LSP) refers to the use of continuous near-infrared lasers to sustain high-density plasmas in high-pressure rare gases, thereby forming a broadband light source for rapid optical defect detection in semiconductor wafers.[1–4] The LSP functions as a broadband plasma light source characterized by high brightness, exceptional stability, and a long operational lifetime exceeding 10^4 hours. Currently, the feature sizes of wafer defects have developed to be smaller than 10 nm, and the stability of the plasma directly determines the quality of the light source output, which in turn affects the accuracy and efficiency of defect detection.[5] Among the factors influencing plasma stability, Zimakov *et al*. believe that the convection around the plasma is the main cause of instability. They observed pressure-related fluctuations in plasma brightness and, using schlieren method, discovered the presence of periodically rising hot gas bubbles around the plasma, proposing a preliminary physical model.[6,7] While Kotov *et al*. used a thermal source to simulate the plasma in fluid dynamics studies and found that the periodic formation and evolution of the surrounding airflow is similar to the shear flow convection heat transfer observed in laminar oscillating flames, exhibiting Kelvin–Helmholtz instability.[8] Liu *et al*. employed a two-dimensional laser-thermal-hydrodynamically coupled fluid model and discovered that plasma is more prone to irregular temporal shape changes when subjected to larger flow field velocities in annular beams.[9,10] KLA-Tencor has attempted to introduce designs such as reverse vortex gas cavities and vortex axes into cavity schemes to mitigate local overheating phenomena that may occur in closed cavities under high-power conditions.[11,12] In our previous work, xenon (Xe) plasma was sustained using continuous fiber lasers in the horizontal direction. We found that tightly focused systems favor plasma stability, and the plasma's center of mass, size, and brightness are all influenced by convection, resulting in uniform frequency fluctuations.[13]

To further investigate the stability of LSP, the laser incident direction was varied under a tightly focused system. The plasma was sustained in the vertical direction from both above and below and compared with the horizontal plasma. Plasma images captured by a high-speed camera were used to calculate the motion patterns as well as the standard deviations of the center of mass and size. Photodetectors and piezoelectric thin-film sensors were employed to measure plasma brightness and internal gas pressure fluctuation. The Schlieren method was used to observe the periodic upward circulating hot gas bubbles around the plasma. A detailed description and quantitative comparison of the characteristics of plasmas sustained

[†]Corresponding author. E-mail: xbwang@hust.edu.cn

© 2026 Chinese Physical Society and IOP Publishing Ltd. All rights, including for text and data mining, AI training, and similar technologies, are reserved.

by lasers in different directions have been conducted. Finally, from the perspective of hydrodynamics, the types of gas flow surrounding the plasma were analyzed, and potential instabilities in gas motion were explored, providing an explanation for the differences in the stability of plasmas sustained by lasers in different directions. Combining experimental and theoretical approaches, this study aims to explore the conditions for achieving a more stable plasma.

2. Experimental setup

After electrode excitation of a traditional short-arc xenon lamp (Model XHA250/T), a continuous fiber laser (Model RFL-C300L) was incident in different directions to sustain high-density Xe plasma in a high-pressure xenon lamp. The experimental setup is shown in Fig. 1. In Fig. 1(a), the continuous fiber laser is incident in the horizontal direction, with a wavelength of 1080 nm and a maximum power of 250 W. L_1 and L_2 form a 2X beam expander, while L_3 is a focusing lens with a focal length of 35 mm. The focusing system has an F-number of 3.5, and the Xe plasma sustained by the laser is located between two electrodes. The initial laser spot diameter was 5 mm, and with a focusing system of $F = 3.5$, the focused spot diameter was 6.26 μm, resulting in a focused spot area of 3.08×10^{-7} cm^2. A high-speed camera (Model AI-030U780M) was used to capture images of the plasma, recording changes in its shape and size. A photodetector (Model DET100A/M) measured fluctuations in the plasma's luminous intensity. A piezoelectric thin-film sensor (Model LDTO-028K) was placed against the outer wall of the lamp to detect changes in the wall pressure, thereby reflecting fluctuations in the gas flow surrounding the plasma.

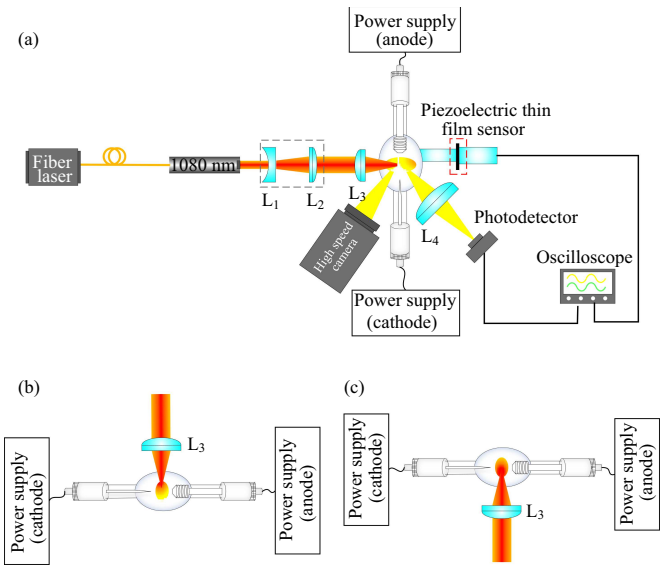


Fig. 1. Experimental setup for Xe plasma sustained by lasers from different directions. (a) Horizontal laser incidence and plasma diagnostics. (b) Plasma sustained by a laser incident from above. (c) Plasma sustained by a laser incident from below.

The light intensity and fluctuation signals were simultaneously displayed on an oscilloscope. To investigate the effect of laser incidence direction on plasma characteristics, the xenon lamp was reoriented from the vertical to the horizontal position. The laser was then aligned vertically to irradiate the plasma from above and below, as shown in Figs. 1(b) and 1(c), respectively. The same diagnostic techniques outlined in Fig. 1(a) were used to analyze the plasma properties under these conditions.

3. Experimental results of stability of laser sustained Xe plasma

3.1. Stability of plasma centroid and size

High-speed imaging of the plasma was performed to investigate the stability of its position and size. The camera was set to capture 1000 frames per second for a duration of 5 seconds, resulting in approximately 5000 images. The plasma shape was fitted using the second-moment method, which was employed in our previous work.[14] The first moment of the plasma intensity corresponds to its center of mass, while the second moment is used to determine its diameter. Figure 2 shows the plasma images sustained by the laser under the following conditions: (a) horizontal incidence, (b) laser incident from top, and (c) laser incident from bottom, at $F = 3.5$ and $P = 250$ W. The laser is incident along the axial direction, with the vertical laser direction being radial, and the horizontal incident laser direction is from right to left. The plasma elongates along the laser propagation direction. The plasma at the laser entrance absorbs a significant amount of laser energy, resulting in a larger plasma shape at the entrance and a gradually tapered tail. The plasma shapes sustained by lasers incident from top and bottom are essentially horizontally symmetric, with the main difference being that the plasma sustained by the laser incident from below has a slightly larger high-temperature region internally.

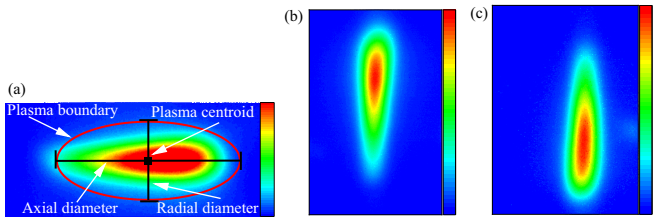


Fig. 2. Plasma sustained by lasers from different directions. (a) Horizontal laser incidence (from right to left), (b) laser incident from top, (c) laser incident from bottom.

The threshold power to sustain plasma differs depending on the direction of the incident laser. The threshold laser power for plasma sustained by lasers incident from the horizontal direction and from the bottom is similar, at 71 W and 64 W, respectively. However, for lasers incident from the top, a laser power of up to 110 W is required to sustain the plasma. When the laser power is below 110 W, the plasma only exists for a brief period of a few seconds, during which its shape and

size become increasingly unstable until the plasma is extinguished. This behavior is related to the thermal gravity convection surrounding the plasma. Periodic upward hot gas bubbles exist around the plasma (as shown in Fig. 6), and these upward-moving hot bubbles interfere with the laser incident from the top, negatively impacting the stability and focus of the laser. Consequently, higher laser power is needed to sustain the plasma.

As the laser power increases, the axial diameter of the plasma gradually expands and moves in the direction of the laser incidence. Figure 3 compares (a) axial diameter and (b) axial center-of-mass displacement of the plasma sustained by lasers from different directions. The plasma sustained by lasers incident from the bottom exhibits the largest axial diameter, while the plasma sustained by lasers incident from the top has the smallest axial diameter. Conversely, the displacement of the plasma follows the opposite trend. As the laser power increases, the plasma sustained by lasers incident from the top moves the furthest. This behavior is attributed to the presence of thermal convection. For plasma sustained by lasers incident from the bottom, the plasma moves downward, and its shape is gradually elongated by the upward thermal airflow. The upward thermal bubbles also hinder the downward movement of the plasma's center of mass. In contrast, for plasma sustained by lasers incident from the top, the gas flow restricts the plasma's lengthening while promoting its movement. This phenomenon is consistent with the conclusion that forced convection in the direction of laser propagation aids in sustaining the plasma at the laser focus position.[15] For plasma sustained by horizontal lasers, the upward thermal convection has a more significant effect on its radial characteristics. As the laser power increases, the radial centroid of the horizontal plasma shifts by 0.03 mm, while the radial center-of-mass shift of the vertical plasma is an order of magnitude less.

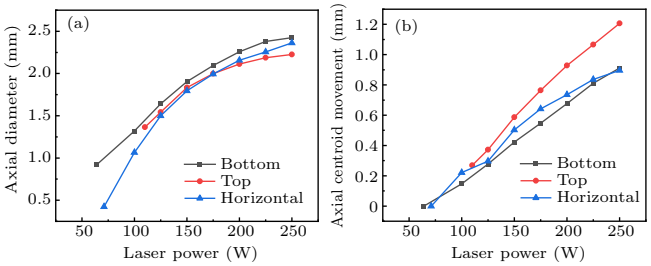


Fig. 3. (a) Axial diameter and (b) axial centroid movement of plasma.

The position and size of the plasma exhibit fluctuations, with the center of mass continuously vibrating and the diameter undergoing expansion and contraction. In the recorded plasma videos, the plasma sustained by lasers incident from the top shows greater instability, with the center of mass and diameter undergoing noticeable and large fluctuations. The standard deviations of the axial center of mass and axial diameter for plasmas sustained by lasers from different directions are compared in Fig. 4.

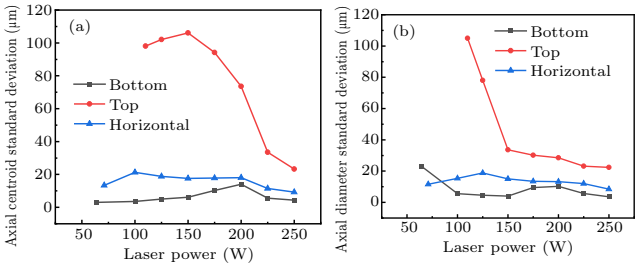


Fig. 4. Standard deviations of axial centroid and axial diameter of plasma.

The standard deviation for the plasma sustained by lasers incident from the top is significantly larger than for the other two cases. The standard deviations for the plasmas sustained by lasers incident from the bottom and from the horizontal direction are similar, but overall, the plasma sustained by lasers incident from the bottom exhibits higher stability. For example, when the laser power is $P = 250$ W, the standard deviations of the axial center of mass for plasma sustained by lasers incident from the top, bottom, and horizontally are 23.27 μm, 9.22 μm, and 4.34 μm, respectively. The standard deviations of the axial diameter are 22.4 μm, 8.5 μm, and 3.54 μm, respectively. As the laser power increases, the standard deviations of the plasma decrease, indicating improved stability. Our results are consistent with the simulation results by Raizer *et al.*, which show that plasma sustained by lasers incident from the bottom has better stability, and that reduced laser power leads to decreased stability.[16]

3.2. Fluctuations in plasma brightness and gas pressure

The light emitted by the plasma also exhibited slight flickering. We used photodetectors to measure the luminous intensity of plasma sustained by lasers from different directions. Simultaneously, a piezoelectric thin-film sensor, positioned against the outer wall of the lamp via a glass rod, was employed to detect changes in the gas pressure on the lamp's outer wall caused by the convection surrounding the plasma. Both the plasma luminous signal and the piezoelectric signal were simultaneously captured and stored using an oscilloscope. Figure 5 shows the brightness signals and convective signals, along with their corresponding frequency spectra, for plasma sustained by lasers at $P = 250$ W from different directions. Figures 5(a)–5(d) represent the plasma sustained by lasers incident from the top, while Figs. 5(e)–5(h) represent the plasma sustained by lasers incident from the bottom. The shapes and fluctuations of the brightness signals and convective signals are largely consistent. Notably, the amplitude of brightness and convective fluctuations is more pronounced in the case of plasma sustained by lasers incident from the top, indicating that the plasma sustained by lasers incident from

the bottom is more stable. This observation is consistent with the trends of standard deviations in plasma size and center of mass discussed in Subsection 3.1. Fourier spectral analysis of the brightness and convective signals reveals a frequency of around 30 Hz, with the same signal frequency observed for the same laser direction. The plasma frequencies differ slightly for different laser directions, with plasma sustained by lasers incident from the bottom exhibiting a lower frequency. This is because, under the influence of thermal convection, the plasma shapes and high-temperature regions differ slightly for lasers incident from different directions, leading to variations in the thermal exchange with the surroundings.

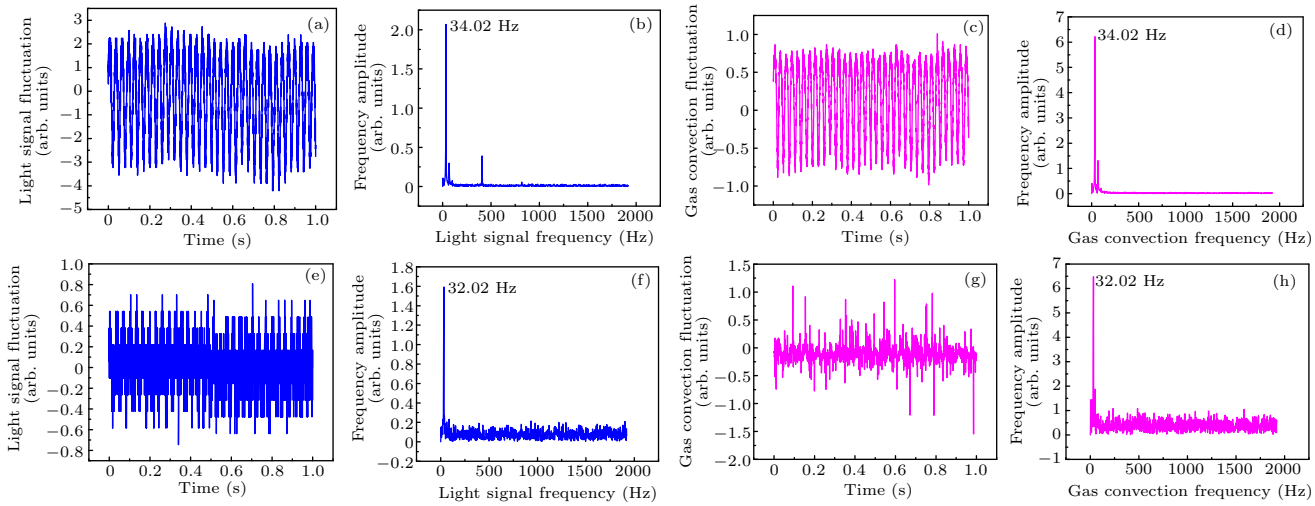


Fig. 5. The laser is incident from top (a) plasma brightness, (b) spectrum, (c) airflow fluctuation, (d) spectrum. The laser is incident from bottom (e) plasma brightness, (f) spectrum, (g) airflow fluctuation, (h) spectrum.

3.3. Schlieren imaging of LSP

To systematically investigate the influence of thermal buoyancy convection on laser-sustained plasma stability under different laser orientations, schlieren imaging was employed to visualize the thermal flow structures surrounding the plasma, as shown in Fig. 6. Figures 6(a) and 6(b) present the convective patterns under top and bottom laser irradiations, respectively, both acquired at $F = 3.5$ with 125-W laser power. The short-arc xenon lamp's electrodes are positioned at the left and right ends in all images, where the central bright spot represents the plasma. Periodic rising thermal bubbles are observed around the plasma in both laser incidence directions. Figure 6 presents the development of a single cycle of these thermal bubbles, with a frequency consistent with the approximately 30-Hz oscillations observed in the plasma brightness discussed earlier. It is interesting to note that in the Schlieren photos shown in Fig. 6(a), a toroidal vortex (in some photos it is highlighted with a red oval) is clearly visible: the 2nd frame shows clearly the birth of a vortex, the 4th frame shows a formed vortex, and the 5th frame shows the completion of the formation of a vortex. One can see that the process goes through the stages of formation until the 4th frame, with a slight upward displacement and subsequent separation. And Fig. 6(b) shows a similar process.

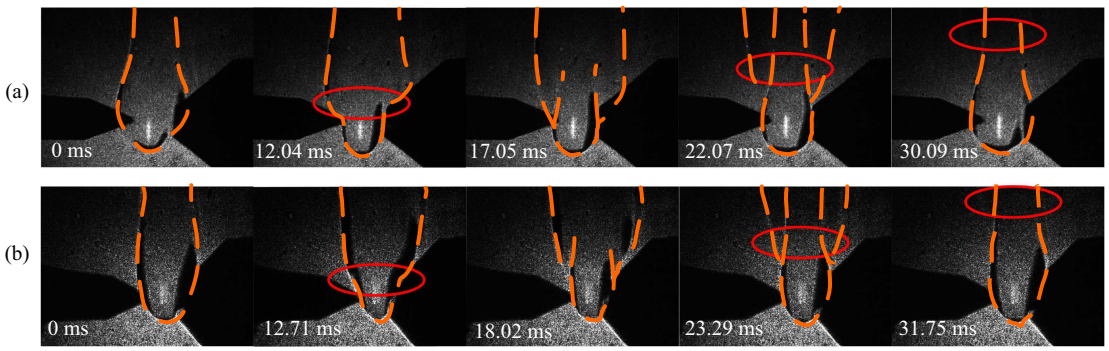


Fig. 6. Hot gas bubble rising around the plasma (a) incident laser (top) and (b) incident laser (bottom).

Although the thermal bubble cycles in the two cases are generally similar, there are still notable differences. As shown in the figure, during one cycle of thermal bubble development, the difference between the maximum and minimum radii of the thermal bubble is larger when the laser is incident from the top. This increases the pressure difference exerted by convection on the bubble wall, resulting in higher signal amplitudes recorded by the piezoelectric film sensor. Mean-

while, when the laser is incident from the bottom, the position and size of the plasma are relatively stable, as evidenced in Fig. 6(b), where the bottom of the thermal bubble remains approximately at the same position throughout the cycle. In contrast, when the laser is incident from the top, as shown in Fig. 6(a), slight vertical oscillations in the position and size of the plasma lead to corresponding vertical shifts in the bottom of the thermal bubble. Regardless of the laser's direction of incidence, the presence of gravity causes the thermal bubbles to rise vertically.

4. Theoretical analysis and discussion of plasma instabilities

During laser-sustained plasma formation, the absorption of laser energy and its conversion into thermal energy create localized high-temperature regions. This process induces a thermodynamic response in the surrounding gas: the gas density in the high-temperature zone decreases, generating buoyancy under gravity and driving upward thermal convection. In a confined space, the gas flow velocity field is governed by the Navier–Stokes equations, often leading to the formation of complex vortex structures. The high-temperature gas rises vertically along the plasma boundary, forming a thermal plume. The ascending flow is then deflected by the upper bulb wall, spreading radially and forming a toroidal vortex. As the gas cools, its density increases, causing it to sink along the periphery and establish a closed circulation loop. Furthermore, the restricted expansion of gas due to the enclosed cavity shifts the dominant convection mode from plume-driven to circulation-driven. Therefore, a theoretical analysis of the flow instabilities around the plasma is essential.

4.1. Instability by the transition of laminar flow to turbulent flow

Usually the Reynolds number Re is used to characterize the flow of a fluid. Let us consider the flows formed in the plasma from the point of view of hydrodynamics. Here are some data that are necessary for further consideration.

Xenon density at the pressure P_{Xe} and the temperature T is as follows:

$$\rho_{\mathrm{Xe}} = 5.9\frac{P_{\mathrm{Xe}} \times 273}{T}. \tag{1}$$

Given that the high-temperature environment surrounding the plasma can reach approximately 10^4 K, the internal pressure of the xenon lamp may attain 5 MPa, at which point the xenon gas density is 8.1 kg/m^3. The temperature-dependent dynamic viscosity of xenon, $\mu_{\mathrm{Xe}}(T)$, at 5 MPa has been documented in prior literature. At a temperature of 10^4 K, the viscosity of xenon gas is approximately 3×10^{-4} kg/(m·s).

The ellipsoidal bulb structure is simplified as a "round flooded jet," with its characteristic dimension defined by the diameter[17,18] and the beginning of the jet in the centroid region. The width of the laser sustained plasma in the horizontal direction is approximately 0.3 mm. Schlieren imaging reveals that gas convection around the plasma primarily occurs between two electrodes. Therefore, the electrode gap of 2 mm is chosen as the diameter for this model. Consequently, the Reynolds number Re is determined as

$$\mathrm{Re}_{\mathrm{Xe}}(T) = \frac{\rho_{\mathrm{Xe}}(T) V_{\mathrm{Xe}} d_{\mathrm{Re}}}{\mu_{\mathrm{Xe}}(T)} = \frac{403}{T\mu_{\mathrm{Xe}}}. \tag{2}$$

Therefore, the Reynolds number of Xe at different temperatures calculated with the help of Eq. (2) is shown in Fig. 7.

As illustrated in Fig. 7, the minimum Reynolds number is $\mathrm{Re}_{\mathrm{Xe}}^{\mathrm{min}} \approx 120$, corresponding to a temperature $T = 1.3 \times 10^4$ K. At $T = 10^4$ K, the Reynolds number increases to 134. For a "round flooded jet," the critical Reynolds number $\mathrm{Re}_{\mathrm{cr}}$ marks the transition from laminar to turbulent flow. Under the experimental conditions of this study, the temperature of the laser-sustained plasma (LSP) remains below 10^4 K, yielding Reynolds numbers exceeding 134. According to Refs. [17–19], when the Reynolds number falls within the range of 100–200, the transition length from laminar to turbulent flow is approximately 1 mm–3 mm. Consequently, the gas flow above the plasma region exhibits pronounced turbulent characteristics. Furthermore, buoyancy effects induce a net upward time-averaged mass flow velocity. Thus, the stability of the laser-sustained plasma irradiated from top is inherently compromised.

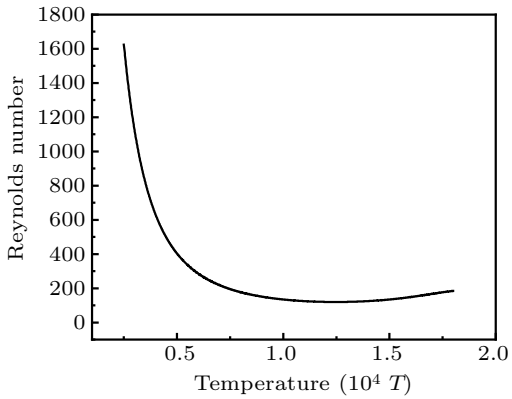


Fig. 7. Reynolds number of Xe at different temperatures.

In our previous work, it was observed that as the laser power increases, the plasma temperature rises from 0.5 eV to 0.9 eV.[20] Within this range, the Reynolds number gradually decreases and stabilizes, indicating an improvement in plasma stability. This is consistent with the trend observed in Fig. 4, where the standard deviations of the centroid and diameter exhibit similar behavior.

4.2. Kelvin–Helmholtz instability in LSP

Meanwhile, Kotov *et al.* suggested that low-frequency modulation of the LSP radiation intensity is caused by the

periodic formation and subsequent breakage of the Kelvin–Helmholtz toroidal vortex covering the volume of the heated gas. The authors suggested that these fluctuations are caused by the periodic appearance of plasma-heated gas in the form of a "bubble". When estimating the frequency of this periodic process, the authors proposed estimating it by the time of expansion (and simultaneous ascent) of the heated gas region from radius r_0 to radius $2r_0$, where r_0 is the radius at which the expansion velocity V_t of the region is equal to the ascent velocity V_i

$$\begin{aligned} f_{pl} &= \frac{V_t(2r_0)}{r_0}, \quad V_i = \sqrt{2rg}, \\ V_t &= \frac{QM_{Xe}}{2\pi c_p r^2 \rho_{Xe}(T_1)(T-T_1)}, \quad V_i(r_0) = V_t(r_0), \\ r_0 &= 2^{-0.2} g^{-0.2} A^{0.4}, \quad A = \frac{QM_{Xe}}{2\pi c_p \rho_{Xe}(T_1)(T-T_1)}, \end{aligned} \tag{3}$$

where Q is the power dissipated in the heating area, which is spent specifically on heating the gas; M_{Xe} and ρ_{Xe} are the atomic mass (in atomic units) and xenon density, respectively; T, T_1 are the temperatures of the heated area of the gas and the gas surrounding this area, respectively; $c_p/M_{Xe} = C_p$ is the specific heat capacity of xenon at constant pressure.[8]

The estimation results demonstrate that the calculated fluctuation frequency closely matches the experimentally observed frequency. The expression for frequency f_{pl} in Eq. (3) can be further simplified and reformulated to calculate the fluctuation frequency f_{fl} of "turbulent flame" radiation (*i.e.*, flickering diffusion flames such as pool fires or low-speed premixed flame combustion: The authors note that equation (3) for the frequency f_{pl} can be reduced to a form that is used to calculate the pulsation frequency f_{fl} of "turbulent flames" radiation (flickering diffusion flames, such as pool flames or premixed flames burning at low feed rates):

$$f_{fl} = \frac{1}{2C}\sqrt{\frac{g}{D}}, \tag{4}$$

where C is a certain constant close to 1 when the flame-heated volume has an upward-converging conical shape; D is the diameter of the Kelvin–Helmholtz toroidal vortex, which periodically (with a frequency of f_{fl}) detaches from the surface of the flame-heated volume.

From Eq. (3) it is easy to find an explicit expression for the pulsation frequency f_{pl}

$$f_{pl} = 2^{-1.4} g^{0.6} A^{-0.2} \approx 1.49 \cdot A^{-0.2}. \tag{5}$$

For $D = 2r_0$ we get $f_{pl} = f_{fl}$. Equation (5) reveals the qualitative dependence of the fluctuation frequency f_{fl} on the dissipated power Q within the heating region; the frequency progressively decreases with increasing Q, a trend consistent with the observed reduction in low-frequency components of both plasma centroid motion and luminosity at higher laser powers. This correlation suggests analogous convective patterns between LSP-driven flows and turbulent flame systems. The similarity further manifests in the morphological characteristics of the heated gas volumes, which in both cases assume an upward-converging conical structure. Consequently, the thermal bubbles surrounding LSPs develop a distinct geometry with a tapered upper region and rounded lower base.

5. Optimization of laser sustained plasma

Stability analysis of plasmas sustained by various laser orientations and focusing configurations revealed that downward laser irradiation combined with a tight-focusing system produces the most stable plasma. Based on this finding, we optimized the optical plasma maintenance system. The experimental setup employed a 4× beam expander to increase the fiber laser beam diameter to 20 mm. This was combined with an aspheric focusing lens having a 16-mm focal length, achieving an F-number of 0.8. The system utilized a domestic 75 W short-arc xenon lamp, model XHA75, featuring a 13-mm outer bulb diameter. The aspheric lens's 7.3-mm back focal length enabled precise positioning of the laser focus between the lamp's two electrodes. High-speed imaging of downward-irradiated plasma at $F = 0.8$ demonstrated nearly circular plasma morphology across various laser power levels, as shown in Fig. 8. In our experiments, under conditions capable of sustaining the plasma, the plasma was sustained continuously and stably as long as the laser remained operational. The plasma exhibited only minimal size variation with increasing power, confirming the tight-focusing system's capability to effectively limit plasma elongation, in agreement with fundamental plasma confinement theory.

Figure 9 presents a comprehensive analysis of plasma stability under varying laser power conditions. The dimensional evolution data in Fig. 9(a) demonstrate controlled plasma expansion, with axial diameter increasing from 0.65 mm to 0.96 mm and radial diameter from 0.69 mm to 0.89 mm as laser power escalates. The system sustains remarkable geometric stability, evidenced by a minimal axial centroid displacement of 0.19 mm and well-regulated aspect ratio variation between 0.94 and 1.07. These measurements confirm the $F = 0.8$ optical configuration's superior capability for generating compact, spatially stable plasmas with near-ideal circular symmetry. The stability metrics presented in Fig. 9(b) reveal significant performance improvements through precision measurements. At 250-W input power, the system achieves sub-micron stability levels, with axial centroid standard deviation of 2.26 μm, radial centroid deviation of 0.93 μm, axial diameter variation of 2.23 μm, and radial diameter variation of 1.73 μm. These values represent substantial enhancement

over all previously tested focusing configurations. Supporting photodiode measurements of plasma emission intensity show markedly reduced fluctuation amplitudes and complete suppression of low-frequency spectral components. These observations collectively indicate a transition toward thermodynamic equilibrium, driven by three interconnected physical mechanisms: elevated plasma temperature conditions, reduced Reynolds number flow characteristics, and enhanced thermal power dissipation within the plasma volume. The experimental results conclusively demonstrate the optimized system's ability to sustain exceptionally stable plasma conditions across all measured parameters.

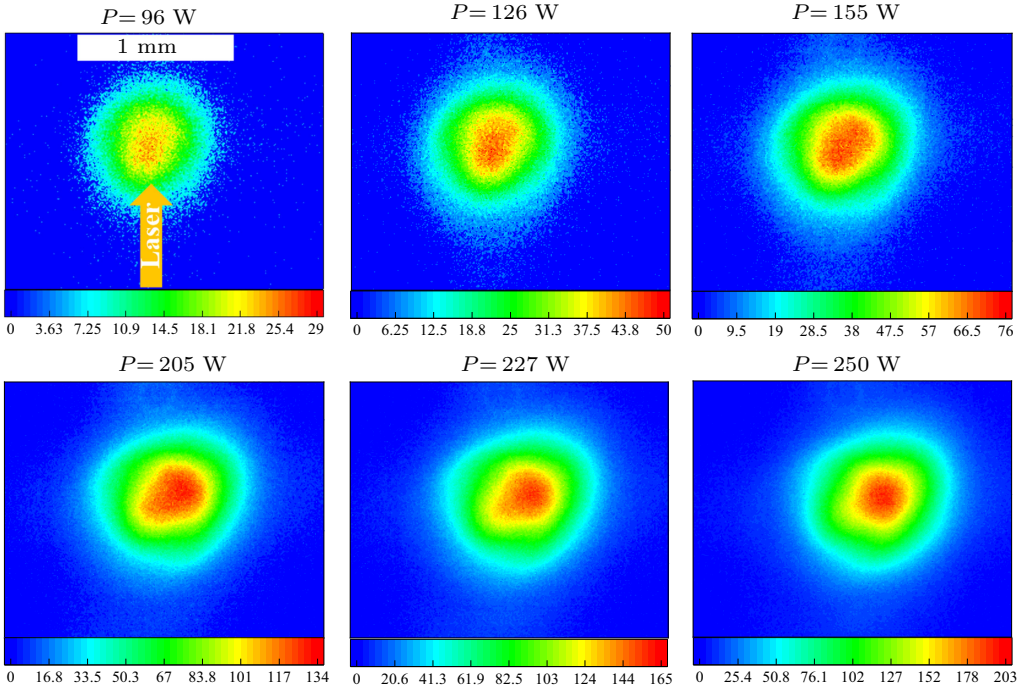


Fig. 8. Plasma images at different laser power levels with bottom laser irradiation and $F = 0.8$.

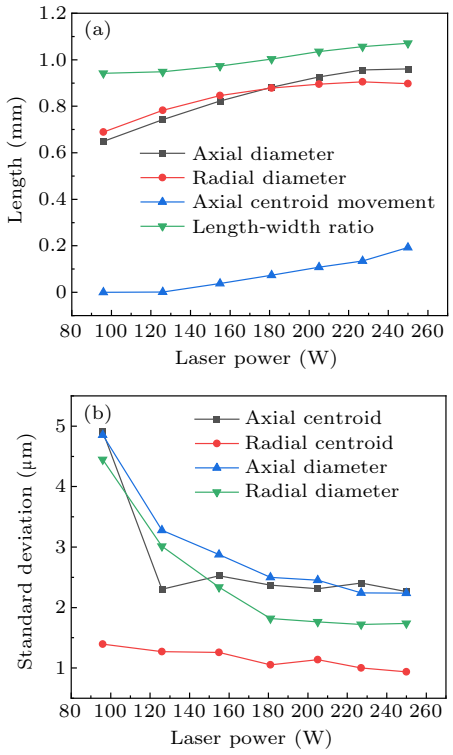


Fig. 9. Plasma characteristics under varying laser power with bottom irradiation at $F = 0.8$: (a) diameter, centroid displacement, and aspect ratio; (b) standard deviations of diameter and centroid position.

Figure 10 displays the centroid scatter plot of a laser-sustained xenon plasma where the laser is incident from below with $F = 0.8$ at $P = 250$ W. The plasma exhibits axial centroid fluctuations of ± 8 μm and radial variations of ± 3 μm. Compared to the horizontally irradiated plasma with $F = 3.5$ at the same power level, this configuration with laser incidence from below and tighter focusing demonstrates superior stability, as reflected in the significantly smaller centroid displacements.

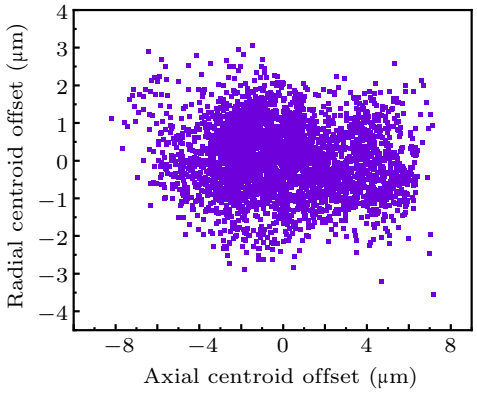


Fig. 10. Centroid scatter plot of plasma at $F = 0.8$ and $P = 250$ W.

The plasma spectrum under the $F = 0.8$ condition was acquired using a miniature fiber optic spectrometer (Ocean Optics, USB2000+ model) with an integration time set to 3 ms. Figure 11(a) presents the processed LSP spectrum cov-

ering the wavelength range of 350 nm–1021 nm. A significant increase in the intensity of the continuous spectrum below 750 nm was observed with increasing laser power, which gradually surpassed the intensity of the line spectra in the longer wavelength region. To extend the spectral range of the plasma to shorter wavelengths, measurements were performed using an OTO Photonics HB1034-FUV2A spectrometer with an integration time of 150 ms. The spectrum covering 180 nm–500 nm is presented in Fig. 11(b). The plasma exhibits strong emission below 350 nm, with a sharp decline in intensity occurring below 225 nm. This attenuation is attributed to the synthetic fused silica envelope of the commercial xenon lamp, which is designed to be ozone-free and consequently has very low transmittance for wavelengths below 250 nm. Compared with the spectrum of a standard 75-W commercial short-arc xenon lamp, the LSP demonstrates significantly higher spectral intensity with increasing laser power.

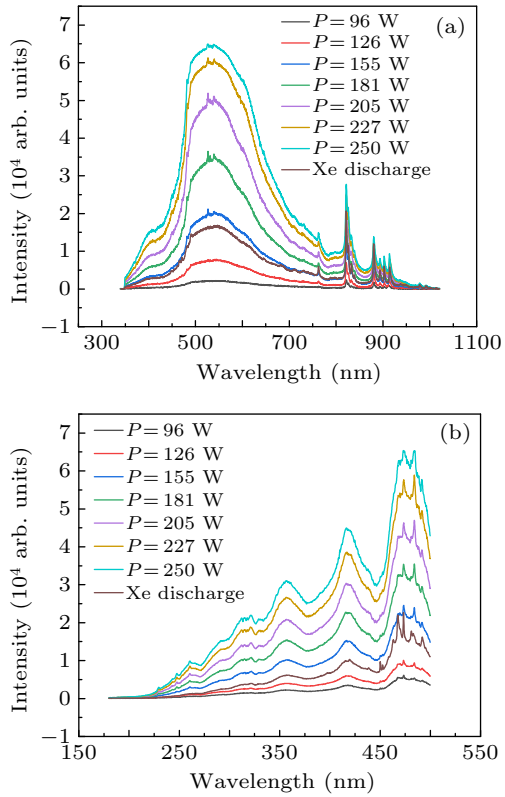


Fig. 11. Plasma spectra at $F = 0.8$: (a) full-waveband spectra and (b) short-wavelength spectra.

6. Conclusion

The characteristics of plasmas sustained by incident lasers from different directions were compared through a combination of experimental and theoretical analyses. A focused continuous-wave fiber laser was vertically incident into a high-pressure xenon lamp from both the top and bottom to sustain high-density plasma. The plasma sustained by the top-incident laser exhibited a higher laser power threshold, larger standard deviations in the plasma centroid position and axial diameter, and significant amplitude fluctuations in light intensity. These instabilities were attributed to periodically rising thermal bubbles surrounding the plasma.

Fluid dynamic analyses were conducted to assess possible reasons for instability occurrence. Firstly, calculating the Reynolds number, we could state that the plasma below the centroid point was more stable due to its laminar motion, while the plasma motion above the centroid point was turbulent. This makes the plasma sustained by the bottom-incident laser more stable. Secondly, we considered the Kelvin–Helmholtz instability and showed without a doubt that this kind of instability, connected with the formation of vortices, explained the occurrence of LSP instability under our conditions.

Based on the aforementioned analysis, the LSP system configuration was optimized by implementing a bottom-incident laser beam with tighter focusing ($F = 0.8$), resulting in a plasma with near-unity aspect ratio (≈ 1) and enhanced stability. At 250-W laser power, the system achieved remarkable stability metrics: 2.26-μm standard deviation in axial centroid position and 2.23-μm standard deviation in axial diameter. These findings establish both experimental and theoretical foundations for developing high-stability LSP light sources. However, under the current experimental conditions, the stability and spectral width of the LSP source have not yet reached the level of commercial products available from manufacturers such as Energetiq and KLA. Further optimization of the plasma characteristics through improved experimental parameters is an objective for future work.

Acknowledgement

Project supported by the Fundamental Research Funds for the Central Universities (Grant No. 2026HUST-SPBU RSFO3).

References

[1] Halder S, Truffert V, Van den Heuvel D, Leray P, Cheng S, McIntyre G, Sah K, Brown J, Parisi P and Polli M 2015 26*th Annual SEMI Advanced Semiconductor Manufacturing Conference (ASMC)*, May 3–6, 2015, Saratoga Springs, NY, USA, p. 19

[2] Shi Z, Yang S, Hu H, Lei H, Yang Z and Yu X 2024 *Light. Sci. Appl.* **13** 274

[3] Yang S, Shi Z, Yu F and Yu X 2023 *Opt. Express* **31** 25625

[4] Sah K, Halder S, Cross A and Leray P 2020 *IEEE Transactions on Semiconductor Manufacturing* **33** 23

[5] Zhu J, Liu J, Xu T, Yuan S, Zhang Z, Jiang H, Gu H, Zhou R and Liu S 2022 *International Journal of Extreme Manufacturing* **4** 032001

[6] Zimakov V, Lavrentyev S, Solovyov N, Shemyakin A and Yakimov M 2019 *Physical-Chemical Kinetics in Gas Dynamics* **57** S84

[7] Kotov M A, Lavrentyev S Y, Solovyov N G, Shemyakin A N and Yakimov M Y 2020 *Journal of Physics: Conference Series* **1675** 012073

[8] Kotov M A, Lavrentyev S Y, Shemyakin A N, Solovyov N G and Yakimov M Y 2022 *Plasma Sources Sci. Technol.* **31** 124002

[9] Liu J, Zhang D H Y and Fu Y 2023 *New J. Phys.* **25** 122001

[10] Zhang D H Y, Liu J B and Fu Y Y 2024 *Acta Phys. Sin.* **73** 025201 (in Chinese)

[11] Bezel I, Zvedenuk L B, Stepanov A E and Torkaman A (U.S. Patent) 2023/0053035 A1 [2023-02-16]
[12] Bezel I, Zvedenuk L B, Stepanov A E, KRerikh V and Potapkin B V (U.S. Patent) US11776804 B2 [2023-10-03]
[13] Hu Y, Hao Z, Wang X and Zuo D 2025 *Opt. Laser. Technol.* **184** 112487
[14] Hu Y, Wang X and Zuo D 2022 *Vacuum* **203** 111229
[15] Zimakov V P, Kedrov A Y, Kuznetsov V A, Shemyakin A N, Solovyov N G and Yakimov M Y 2011 *Laser Resonators and Beam Control XIII*, February 18, 2011, San Francisco, California, USA, p. 791305
[16] Raizer Yu P and Surzhikov S T 1990 *Fluid Dynamics.* **24** 593
[17] verák V 2011 *Journal of Mathematical Sciences* **179** 208
[18] Schlichting H 1933 *ZAMM – Journal of Applied Mathematics and Mechanics Zeitschrift für Angewandte Mathematik und Mechanik* **13** 260
[19] Broman G I and Rudenko O V 2010 *Uspekhi Fizicheskih Nauk* **180** 97
[20] Hu Y, Wang X and Zuo D 2024 *Spectrochim Acta Part B At. Spectrosc* **212** 106843